Smith Predictor Controller for Exoskeleton Robot Driven by Electrohydraulic Servo System with Time Delay

Mengdi Su, Lie Yu and Ruifeng Zhao

***Abstract*—Electrohydraulic servo system (EHSS) are usually used to actuate the exoskeleton robots for their abilities to deliver accurate and high power. However, their exists an inevitable time delay for EHSS, because it costs a certain time to make the oil pumped from the tank into the servo and cylinder. To overcome this problem, this paper utilizes the Smith predictor to compensate the time delay. Firstly, the dynamic model is built to compute the desired torque based on the Lagrange equation and fluid equation. The desired torque is transformed into the form of transfer function, and the control law is designed by introducing a time constant. Moreover, this time constant is supposed to be set as the same as the time delay. The results demonstrate that the Smith predictor deeply decreases the time delay and promotes the control performance.**

***Index Terms*—Electrohydraulic servo system, Exoskeleton robot, Smith predictor, time delay.**

I. Introduction

Exoskeleton robots research had contributed to solve some society problems including soldier power augmentation, elderly people rehabilitation training and patient motion assisting [1-2]. The most critical problem for the exoskeleton control is to enable the robot to recognize the human's motion intention such that the robot could synchronize with the human [3]. Electrohydraulic servo system (EHSS) had been widely used to actuate the exoskeleton robot due to their stiffness, fast responses, low cost and high power density [4-5]. According to the control aim, the EHSS can conduct both the position control and force control strategies for the exoskeleton robot. In practice, force control is the most common-used strategy for the exoskeleton robots [6-7]. Conducting force control for EHSS is a great challenge due to the high nonlinearity of dynamic behavior and non-negligible uncertainty of the model parameters [8]. To be specific, the dynamic model involved the discontinuous sign function and square-root function, while the parameters values may vary due to temperature changes and air entrapment in the hydraulic fluid [9].

Manuscript received Jan 10th, 2021; revised Sept 16th, 2021. This work was supported by the National Key R&D Program of China "The study on Load-bearing and Moving Support Exoskeleton Robot Key Technology and Typical Application" (2017YFB1300502). This work was also supported by the National Natural Science Foundation of China (62106178).

Mengdi Su is a student of School of Electronic and Electrical Engineering, Wuhan Textile University, Wuhan, China. (e-mail: md_su1234@163.com)

Lie Yu is a teacher of School of Electronic and Electrical Engineering, Wuhan Textile University, Wuhan, China. (phone: +0086 18607155647; e-mail: lyu@wtu.edu.cn). Lie Yu is the corresponding author.

Ruifeng Zhao is a senior engineer of Wuhan Maritime Communication Research Institute, Wuhan, China. (e-mai: ZHAORUIFENG_WH@163.com)

Generally, the PID controller is vastly used in industrial manufacture because of its simple structure and easy realization [10]. However, the PID controller is not capable of achieving advanced force control for EHSS, as their exist some inevitable limitations such as phase lag, big overshot and independence of model. To overcome these drawbacks, it is necessary to utilize the advanced model-based control schemes such that the Smith predictor could be used to reduce the phase delay and promote the control performance. Giraldo et al designed a filtered Smith predictor to process the control system of multiple inputs and outputs (MIMO) with multiple time delays [11]. This method was based on the decentralized direct decoupling structure through tuning the controller parameters and simplifying the problem to multiple single loops. The simulation results showed that the proposed method could improve the control performance by achieving a decoupled response. Xing et al applied a Smith predictor to compensate for the vehicle actuator delay [12]. A PD controller is conducted on a delay-free vehicle model to make the vehicle follow a desired distance, while the Smith predictor was modified to be robust to the acceleration disturbance. The experimental results demonstrated that the time gap was decreased by more than 15%. Gao et al presented a Smith predictor to reject disturbances for a system with an input time delay and disturbances [13]. However, the time delay was handled by a equivalent input disturbance approach, while the free-weighting matrix approach was used to devise the delay-dependent stability condition in terms of a matrix inequality. The result was evaluated that the proposed method provided satisfactory disturbance rejection performance. Bowthorpe et al utilized a Smith predictor to compensate a time delay between image acquisition and processing for a teleoperated robot [14]. This method aimed to avoid the teleoperated robot's end-effector to collide with the heart. The results suggested that the presented method significantly decreased the mean absolute error and improved the heart motion tracking. In short, the Smith predictor can both reduce the time delay and decrease the disturbance.

This paper is focusing on reducing the time delay for the exoskeleton robot driven by EHSS. The dynamic model is built without time delay based on the Lagrange equation and fluid pressure equation. Meanwhile, the practical system could be considered as the built dynamic model adding the time delay. The Smith predictor is selected to compensate the time delay from the input current to the actuating force of servo valve. To guarantee the whole system stable, the PID controller is combined with the established dynamic model to design the control block. The results are evaluated in terms of the force tracking error and the degree of time delay reduction.

II. DYNAMIC MODEL AND SYSTEM FORMULATION

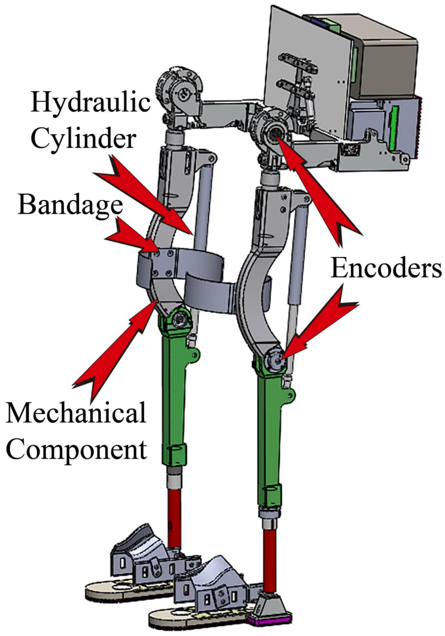

Fig. 1. Schematic structure of the exoskeleton robot.

Fig. 2. Actual effect of people wearing the exoskeleton

As depicted in Figure 1, the EHSS is selected to drive the lower exoskeleton leg. The hydraulic cylinder is mounted between the robotic thigh and shank, and driven by a motion pump. The oil is pumped out from the tank to flow into a servo valve which precisely controls the fluid and pressure inside the cylinder. This paper is focusing on the force control tracking of the knee joint, and Figure 2 shows the real person wearing the exoskeleton robot. The purpose of designing the lower exoskeleton robot is to consume the power as less as possible for human to support the load on the back. As a result, the human dynamic can be described as:

$$T_{HM} = T_d - T_L \tag{1}$$

where T_{HM} is the torque supplied by the human, T_d is desired torque to make the load to move, and T_L is the torque provided by the exoskeleton. T_d can be figured out through the Lagrange equations in the follow.

$$T_d = \frac{d}{dt}\left(\frac{\partial L}{\partial \dot{q}_2}\right) - \frac{\partial L}{\partial q_2} \tag{2}$$

where L is the total energy of the lower exoskeleton leg, and q_2 is the rotary angle of the knee joint. L can be gained below.

$$\begin{aligned} L = &\frac{1}{2} m_t L_t^2 q_1^2 + \frac{1}{2} m_s L_s^2 q_2^2 + \frac{1}{2} I_t q_1^2 + \frac{1}{2} I_s q_2^2 \\ &+ m_t g L_{gt} \cos(q_1) + m_s g L_{gs} \cos(q_1 + q_2) \end{aligned} \tag{3}$$

where m_t is the mass of the robotic thigh, and m_s is the mass of the robotic shank. I_t is the inertia of the robotic thigh, and I_s is the inertia of the robotic shank. L_{gt} is the center of the length of the robotic thigh, and L_{gs} is the center of the length of the robotic shank. q_1 is the rotary angle of the hip joint, and g is the acceleration of gravity. Substituting the Equation (3) into the Equation (2), the desired torque T_d could be computed as:

$$\begin{aligned} T_d = &\frac{1}{2} m_s L_s^2 (\dot{q}_1^2 + 2\dot{q}_1 \dot{q}_2 + \dot{q}_2^2) + m_s L_t L_s \cos(q_2)(L_t^2 \dot{q}_1^2 + L_t L_s \dot{q}_1 \dot{q}_2) \\ &\frac{1}{2} m_s L_t^2 \dot{q}_1^2 + m_s g L_t \cos(q_1) + m_s g L_s \cos(q_1 + q_2) \end{aligned} \tag{4}$$

In order to compute T_d, the rotary angles, velocities and accelerations from robot joints should be acquired. In practice, the encoders are placed severally inside the robotic hip and knee joints to measure the rotary angles, velocities and accelerations. On the other side, T_L is acquired through the modeling of EHSS, and the whole process had been clearly derived in the Reference [15].

$$\begin{cases} T_L = F_L H \\ \dot{F}_L = f_1 i - f_2 v_p - f_3 F_L \end{cases} \tag{5}$$

where F_L is the force generated by the cylinder, H is the arm of length, i is the input current and v_p is the velocity of the hydraulic piston. And the H, f_1, f_2 and f_3 could be described as:

$$\begin{cases} H = \dfrac{r_1 r_2 \sin(q_2 - a\tan(\frac{a}{b}) - a\tan(\frac{d}{c}))}{\sqrt{r_1^2 + r_2^2 + 2r_1 r_2 \cos(q_2 - a\tan(\frac{a}{b}) - a\tan(\frac{d}{c}))}} \\ r_1 = \sqrt{a^2 + b^2} \\ r_2 = \sqrt{c^2 + d^2} \\ f_1 = (\dfrac{R_1}{V_1} + \dfrac{R_2}{V_2})\beta k_q k_c \\ f_2 = (\dfrac{1}{V_1} + \dfrac{1}{V_2}) A_{p1} \\ f_2 = \dfrac{1}{A_{p1}}(\dfrac{1}{V_1} + \dfrac{1}{V_2})\beta C_t \end{cases} \tag{6}$$

where a, b, c and d are the geometric lengths of the robotic structure. Moreover, the schematic diagram of the knee joint is depicted in Figure 3. β is the effective bulk modulus in the cylinder chamber, k_q is the valve discharge gain, k_c is the a positive electrical constant, A_{p1} is the area of the cylinder and C_t is the coefficient of the total internal leakage of the actuator due to the pressure.

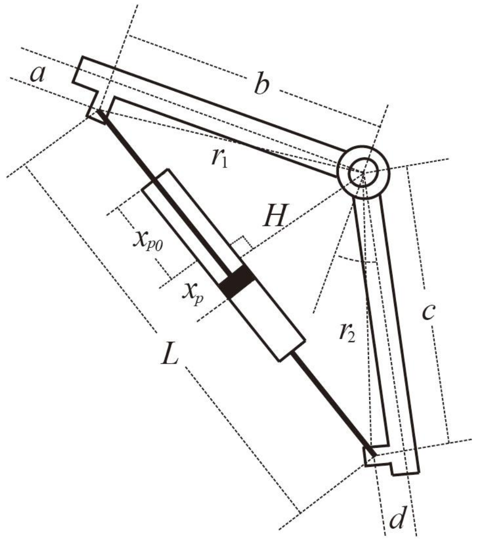

Fig. 3. Numeric description of the robotic knee joint.

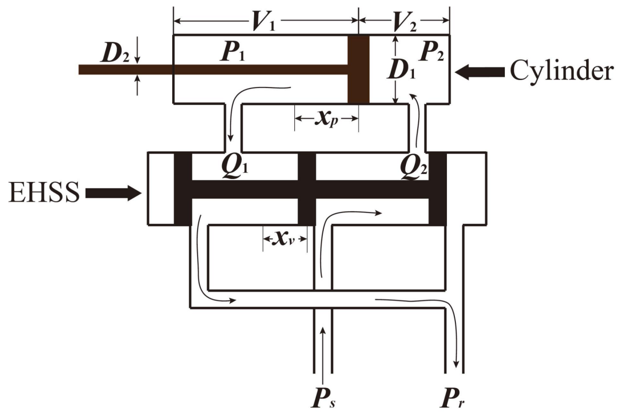

Fig. 4. Schematic diagram of EHSS.

V_1, V_2, R_1 and R_2 could be defined as:

$$\begin{cases} V_1 = V_0 + A_{p1} x_p \\ V_2 = V_0 - A_{p1} x_p \\ R_1 = s(i)\sqrt{P_s - P_1} + s(-i)\sqrt{P_1 - P_r} \\ R_2 = s(i)\sqrt{P_2 - P_r} + s(-i)\sqrt{P_s - P_2} \end{cases} \tag{7}$$

where V_1 and P_1 are the volume and pressure of the cylinder chamber with no rod, while V_2 and P_2 are the volume and pressure of the cylinder chamber with rod. x_p is the displacement of the hydraulic piston. V_0 is a constant volume which meets the condition that x_p=0 and V_1=V_2=V_0. P_s is the supply pressure, and P_r is the return pressure. The schematic diagram of EHSS is clearly described in Figure 4, which plots the oil flowing into the servo valve and cylinder. The function $s(i)$ is defined as:

$$s(i) = \begin{cases} 1, & if\ i \ge 0 \\ 0, & if\ i < 0 \end{cases} \tag{8}$$

The x_p in Equation (7) could be calculated through the Lambert cosine law, while the v_p in Equation (5) is the differential of x_p. Therefore, they could be written as:

$$\begin{cases} x_p = \sqrt{r_1^2 + r_2^2 + 2r_1 r_2 \cos(q_2 - a\tan(\frac{a}{b}) - a\tan(\frac{d}{c}))} - x_{p0} - L_0 \\ v_p = \dfrac{-2r_1 r_2 \sin(q_2 - a\tan(\frac{a}{b}) - a\tan(\frac{d}{c}))\dot{q}_2}{\sqrt{r_1^2 + r_2^2 + 2r_1 r_2 \cos(q_2 - a\tan(\frac{a}{b}) - a\tan(\frac{d}{c}))}} \end{cases} \tag{9}$$

where L_0 is the dead length of cylinder, while x_{p0} is the piston position when the volumes are equal on both cylinder sides. On the other side, the linear acceleration of the hydraulic piston could be approximately modeled as:

$$m_s a_p = m_s \dot{v}_p = m_s \ddot{x}_p = \frac{T_L - m_s g L_{gs} \cos(q_1 + q_2)}{H} \tag{10}$$

where a_p is the acceleration of the hydraulic piston. In practice, the exoskeleton robot is made of lightweight material such that the magnitude of m_s is relatively small. As a result, the Equation (10) could be approximated as:

$$m_s a_p = m_s \dot{v}_p = m_s \ddot{x}_p \approx \frac{T_L}{H} \tag{11}$$

The pressure dynamics of P_1 and P_2 in Equation (7) can be built through the continuity equation proposed by Merritt [16].

$$\begin{cases} \dot{P}_1 = \dfrac{\beta}{V_1}(-A_{p1}v_p - C_t P_L + Q_1) \\ \dot{P}_2 = \dfrac{\beta}{V_2}(A_{p2}v_p + C_t P_L + Q_2) \\ Q_1 = k_q x_v [s(x_v)\sqrt{P_s - P_1} + s(-x_v)\sqrt{P_1 - P_r}] \\ Q_2 = k_q x_v [s(x_v)\sqrt{P_2 - P_r} + s(-x_v)\sqrt{P_s - P_2}] \end{cases} \tag{12}$$

where Q_1 is the supply flow rate to the forward chamber and Q_2 is the return flow rate of the return chamber. x_v is the spool valve displacement of the servo valve.

III. Controller Design

The control aim of the exoskeleton robot is to minimize the torque T_{HM} imposed by human such that the control block could be described in Figure 5. The error e between the desired torque T_d and the actual torque T_L is just the torque T_{HM} defined in Equation (1). The PID controller is selected to control the torque T_{HM} to be closed to zero. The output of the PID controller is the current i (seen in Equation (5)) which enforces the EHSS to actuate the exoskeleton robot. The actual torque T_L is measured through a pull-push sensor, while the desired torque T_d is computed through the dynamic modeling described from Equation (2) to Equation (4). For practical EHSS, there exists a time delay τ because it costs time to pump the oil from the tank into cylinder, and generate the force F_L to push or pull the rod at the meantime. As a result, the controller design should take consideration of the EHSS with time delay.

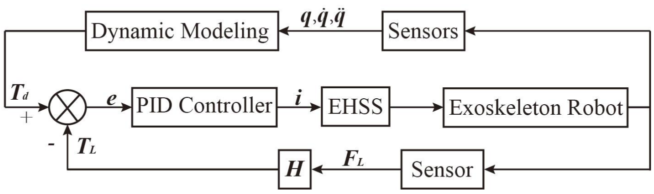

Fig. 5. Control block of the exoskeleton robot.

A. Design of the PID controller

The PID controller is the most widely used controller due to its simple control structure, easy design and independence to the system transfer function. The PID could be established in Figure 5, and the control law can be written below.

$$\begin{cases} i(t) = k_p e(t) + k_i \int e(t)dt + k_d \dfrac{de(t)}{dt} \\ e(t) = T_{HM}(t) = T_d(t) - T_L(t) \end{cases} \tag{13}$$

where k_p, k_i and k_d are the proportional, integral and differential gains, respectively. $e(t)$ is the error between the desired and actual torques. The control aim is to narrow down the error to be zero, while the control law is to adjust the system output according to the change of $e(t)$.

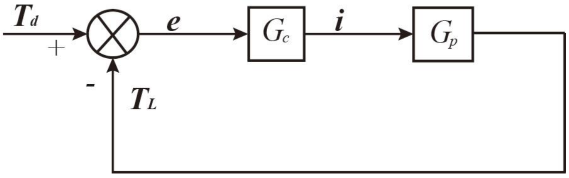

Fig. 6. Description of transfer function for the PID controller.

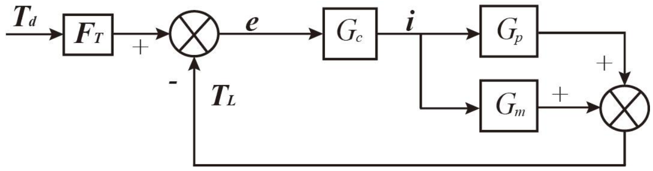

Fig. 7. Description of transfer function for the Smith predictor controller.

B. Design of the Smith-predictor controller

Considering the system transfer function, the control structure in Figure 5 could be restated as the block in Figure 6. G_c is the transfer function of the PID controller, and G_p is the transfer function about the input current and output torque. The input of G_p is the current i, while the output is the actual force T_L. According to the Equation (5) and Equation (11), the G_p could be written in the following.

$$\begin{cases} G_p(s) = \dfrac{T_L(s)}{I(s)} e^{-\tau s} = G_0 e^{-\tau s} \\ G_0(s) = \dfrac{Hf_1}{s^2 + f_3 s + f_2 / m_s} \end{cases} \tag{14}$$

where τ is the time delay, and the G_0 is the ideal transfer function. If the G_c is selected as the PID controller, the control block in Figure 6 is equivalent to the design in Section 3.1. However, the PID controller couldn't remove the effect of time delay. To overcome this drawback, the Smith-predictor control is used to stabilize the time-delay process, and the control block is depicted in Figure 7. The transfer function between the current and the actual torque could be inferred as:

$$\frac{T_L(s)}{I(s)} = G_p + G_m = G_0 e^{-\tau s} + G_m \tag{15}$$

The control aim of Smith-predictor controller is to remove the time delay such that the Equation (15) could be rewritten as:

$$\frac{T_L(s)}{I(s)} = G_0 = G_0 e^{-\tau s} + G_m \tag{16}$$

According to the result in Equation (16), the G_m could be designed as:

$$G_m = G_0(1-e^{-\tau s}) \tag{17}$$

The transfer function between the desired T_d and the actual torque T_L could also be inferred as:

$$\frac{T_L(s)}{T_d(s)} = \frac{F_T G_c(G_p + G_m)}{1+G_c(G_p+G_m)} \tag{18}$$

where F_T is to filter the input signal and make the whole system stable. G_p is the actual transfer function which couldn't be directly obtained, and the actual torque T_L is gained through the measure force F_L times the arm of length H. G_m is the ideal transfer function through mathematical modeling. If the G_m is modeled perfectly such that G_p+G_m=G_0, the Equation (18) could be rewritten as:

$$\frac{T_L(s)}{T_d(s)} = \frac{F_T G_c G_0}{1+G_c G_0} \tag{19}$$

The formation of G_0 is described in Equation (14), and G_c is the controller needed to be designed. The PID controller could also be induced with the result that the G_c could be written as:

$$G_c = K_p(1+\frac{1}{T_i s}+T_d s) \tag{20}$$

where K_p, T_i and T_d are the controller gains. Then, the Equation (19) could be rewritten as:

$$\frac{T_L(s)}{T_d(s)} = \frac{G_c G_0}{1+G_c G_0} = \frac{F_T K_p(1+\frac{1}{T_i s}+T_d s)\frac{m_s H f_1}{m_s s^2 + m_s f_3 s + f_2}}{1+K_p(1+\frac{1}{T_i s}+T_d s)\frac{m_s H f_1}{m_s s^2 + m_s f_3 s + f_2}}$$
$$= \frac{F_T m_s H f_1 K_p(1+T_i s + T_i T_d s^2)}{m_s T_i s^3 + m_s(T_i f_3 + H f_1 K_p T_i T_d)s^2 + (T_i f_2 + m_s K_p T_i H f_1)s + m_s K_p H f_1} \tag{21}$$

The transfer function of the whole exoskeleton robot system is established above. However, the denominator in Equation (21) is a third-order differential equation, and it is important to make the transfer function have a good tracking performance. In order to meet this need, the Equation (21) should be set to be the following form according to the stability acquirement in Reference [13].

$$\frac{T_L(s)}{T_d(s)} = \frac{1}{(\lambda s+1)^3} \tag{22}$$

where λ is a time constant. The Equations (21) and (22) should be equivalent such that the PID parameters should be set as follows.

$$\begin{cases} K_p = \dfrac{3m_s - \lambda f_2}{m_s \lambda H f_1} \\ T_i = 3\lambda^2 m_s - \lambda^3 f_3 \\ T_d = \dfrac{3m_s - m_s\lambda^2 f_3}{3\lambda m_s - \lambda^2 f_2} \\ F_T = \dfrac{1}{T_i T_d s^2 + T_i s + 1} \end{cases} \tag{23}$$

Obviously, the values of the PID parameters and the filter F_T are only relevant to λ with the result that the controller design could be simplified. If λ is set to be equal to the time delay τ, the whole system would gain a good robustness. Additionally, the design of the filter F_T could offset the zero points in Equation (21) and decease the overshot of the system response.

IV. Results

The proposed method is tested via the Matlab software, while the joint rotary angles are extracted from the actual walking of the exoskeleton robot. The parameters of EHSS modeling are listed in Table I, while those for building the robot dynamic are depicted in Table II. To obtain the optimal gains for the PID controller, the Ziegler-Nichols method is selected to optimize the whole control block. Therefore, the best values are figured out that k_p=0.13, k_i=4.13 and k_d=0.04.

TABLE I
SYSTEM PARAMETERS OF EHSS

Name	Symbol	Unit	value
Acceleration due to gravity	g	m/s^2	9.81
Rodless area	A_{p1}	m^2	1.77×10^{-4}
Rod-side area	A_{p2}	m^2	1.57×10^{-4}
Cylinder diameter	D_1	m	0.015
Rod diameter	D_2	m	0.005
Chamber volume	V_0	m^3	1.4×10^{-4}
Effective bulk modulus	β	Pa	2.8×10^7
Coefficient of the total internal leakage	C_t	$m^5N^{-1}s^{-1}$	6.5×10^{-12}
Discharge coefficient	C_d	—	0.61
Spool valve area	w	m^2	9.59×10^{-3}
Valve discharge gain	k_q	m^2s^{-1}	2.87×10^{-4}
Supply pressure of the fluid	P_s	Pa	2×10^6
Return pressure	P_r	Pa	0.5×10^5
Density of hydraulic oil	ρ	$Kg.m^{-3}$	830
Electrical constant	k_c	$m^3s^{-1}Pa^{-1}$	1.38×10^{-4}

TABLE II
SYSTEM PARAMETERS OF THE EXOSKELETON ROBOT

Name	Symbol	Unit	value
Mass of the robotic thigh	m_t	kg	4.235
Mass of the robotic shank	m_s	kg	3.158
Inertia of the robotic thigh	I_t	$N.m$	0.0327
Inertia of the robotic shank	I_s	$N.m$	0.0109
Center of the length of the thigh	L_{gt}	m	0.1588
Center of the length of the knee	L_{gs}	m	0.1134
Length of the mechanical structure	a	m	0.032
Length of the mechanical structure	b	m	0.266
Length of the mechanical structure	c	m	0.039
Length of the mechanical structure	d	m	0.023

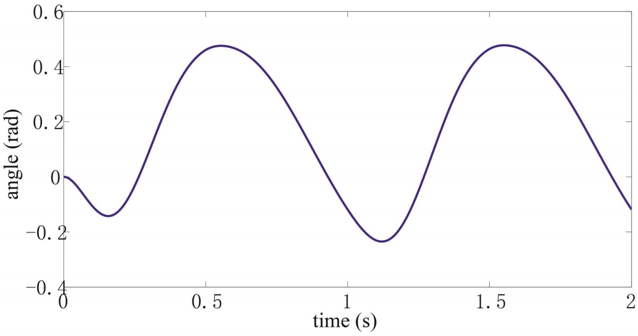

（a） Hip joint motion angle

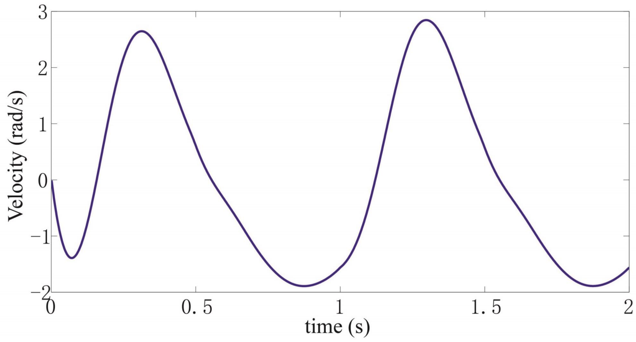

（b） Hip joint motion velocity

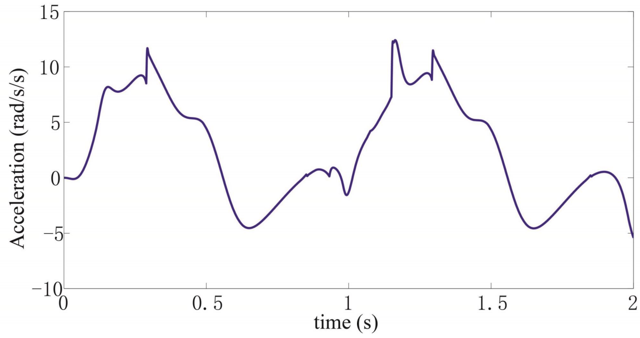

（c） Hip joint motion acceleration

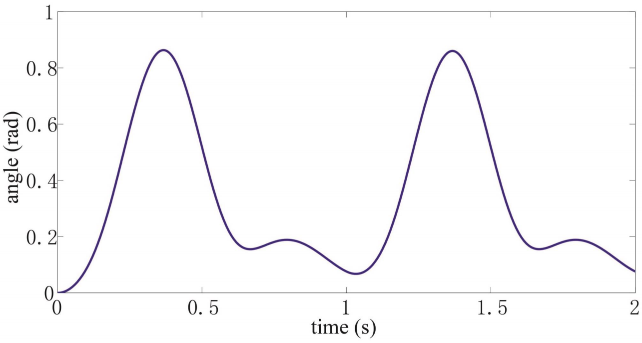

（d） Knee joint motion angle

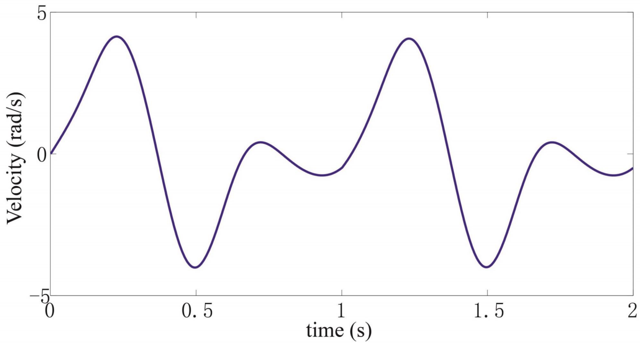

（e） Knee joint motion velocity

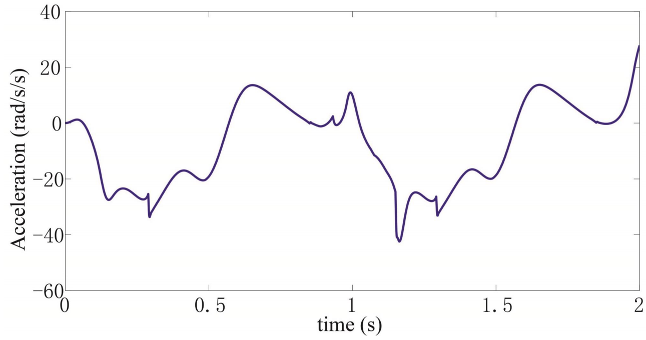

（f） Knee joint motion acceleration

Fig. 8. Joint angles, velocities and accelerations from the robotic joints.

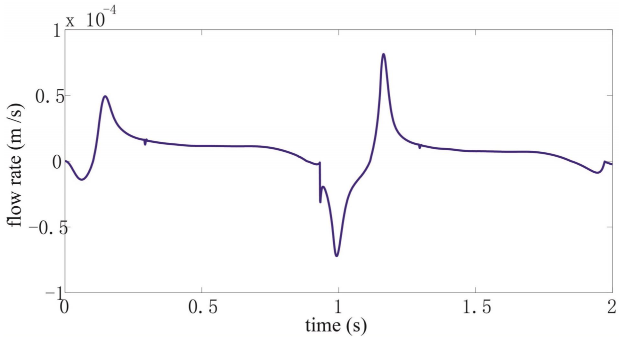

（a） Supply flow rate

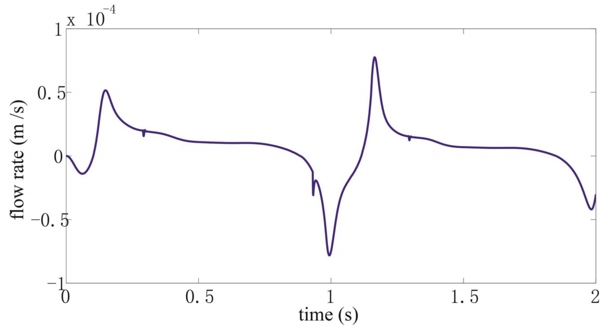

（b） Return flow rate

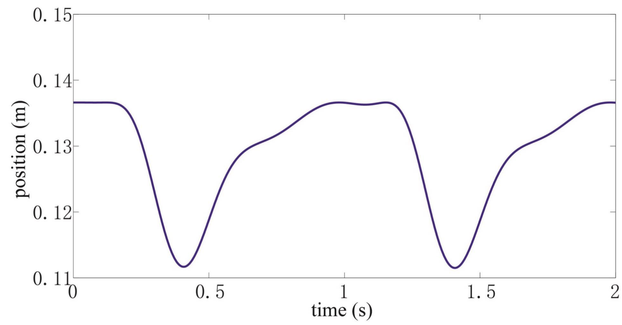

（c） Knee Hydraulic Piston Position

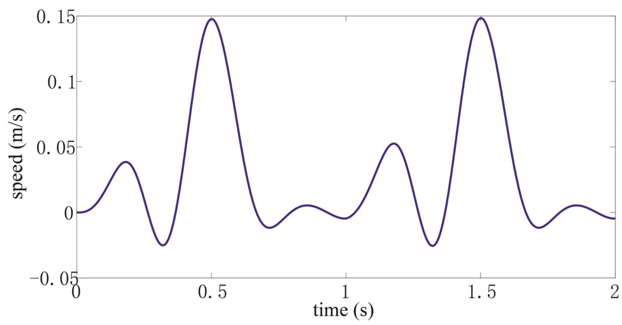

（d） Knee hydraulic piston velocity

Fig. 9. Changes of flow rate and piston motion

The input data including the joint angles, velocities and accelerations were collected from the actual sensors, and pictured in Figure 8. The subject wore the robot to walk on a level ground, while the encoders inside the knee and hip joints recorded these data in real time. The angle, velocity and acceleration of the robotic hip joint are shown in Figure 8(a), (c) and (e), while those of the robotic knee joint are depicted in Figure 8(b), (d) and (f). Then, the robot dynamic could be calculated through the Lagrange equation, and the desired torque could be gained with the result that the control strategy can be realized. Under the control of the Smith predictor, the changes of flow rate and piston motion are monitored and depicted in Figure 9. The Q_1 and Q_2 vary with the spool position (i.e., x_v), and keep the same change trend. Equation (9) defines the computation of piston position (i.e., x_p) and velocity (i.e., v_p), and Figure 9(c) and (d) depict their changes with the joint angle and velocity.

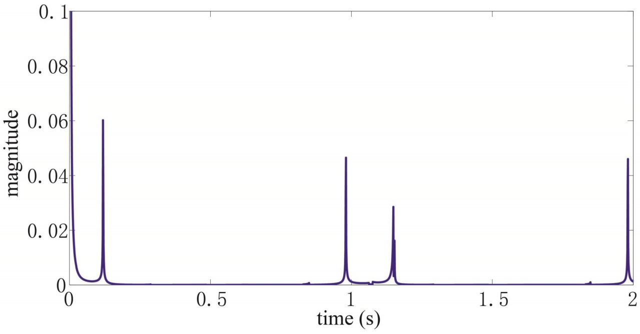

（a）Value of K_p

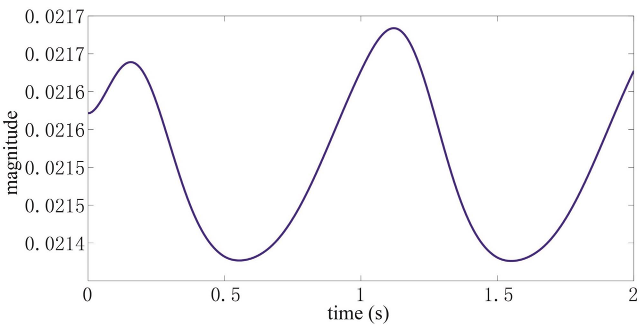

（b）Value of T_i

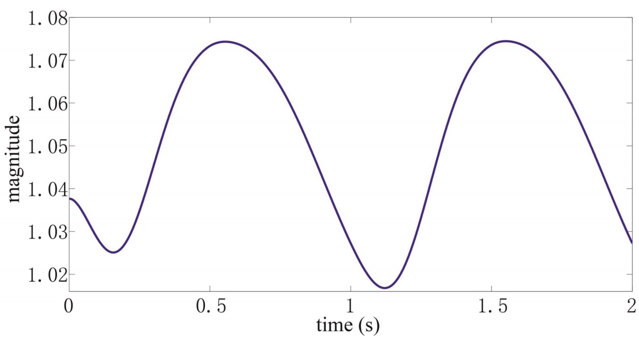

（c）Value of T_d

Fig. 10. Parameter changes of the Smith predictor controller.

According to Equation (23), the controller parameters of the Smith predictor is related to the time constant λ which is supposed to be equal to the time delay τ. In practise exoskeleton system, the time delay is about 0.01 second, and the setting is given that $\lambda = \tau = 0.01$ s. Therefore, the controller parameters of K_p, T_i and T_d are shown in Figure 10(a), (b) and (c), respectively. At most of time, the K_p keeps at a low value, but sometimes varies sharply to adjust the control output. The T_i and T_d are adjusted through the motion change such that the control output would adapt to the walking conditions.

To exhibit the control results, the performances of the PID controller and the Smith predictor controller are compared. Figure 11 depicts the control effect of time delay for the two controllers. It could be obviously analyzed that the time delay is visible for the traditional PID controller as shown in Figure 11(a). However, it is difficult to view the time delay for the Smith predictor as described in Figure 11(b). Figure 12 describes the human-machine torque under the two controllers, while the human-machine torque is defined as the error between the desired and actual torques. Obviously, the Smith predictor controller gains smaller human-machine torque compared with the PID controller. The comparative results reveal that the Smith predictor controller narrows down the time delay more clearly than the PID controller, and completes the control aim better.

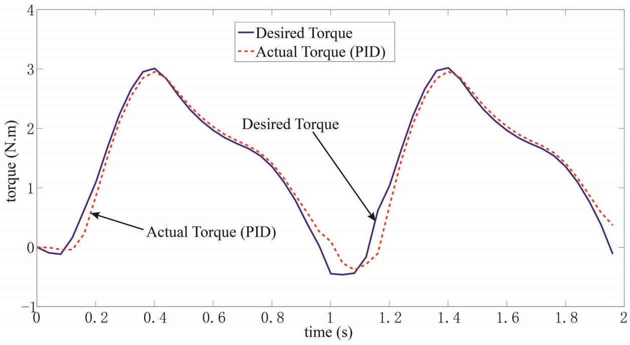

（a）Control effect of the PID controller

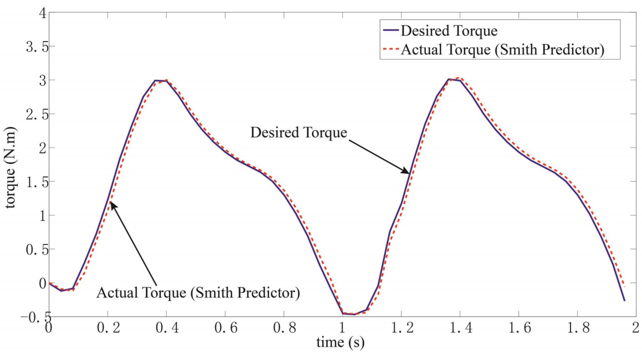

（b）Control effect of the Smith predictor controller

Fig. 11. Comparison of torque tracking control between the PID controller

and the Smith predictor controller.

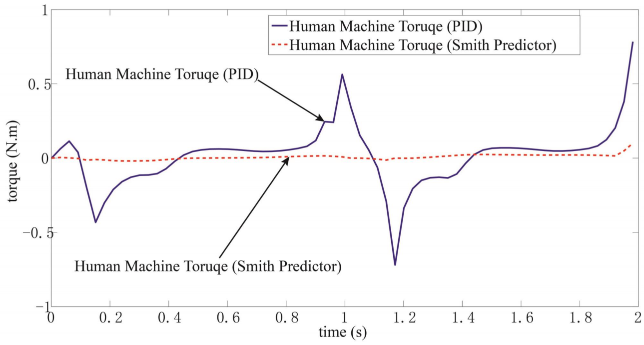

Fig. 12. Comparison of human-machine torque between the PID controller and the Smith predictor controller.

TABLE III
QUANTITATIVE COMPARISON FOR TWO CONTROLLERS

Controllers	PID Controller	Smith Predictor Controller
Time Delay	0.011 s	0.001 s
MAE	0.0674 N.m	0.0235 N.m

In order to make the results more explicit, quantitative analysis is provided to digitalize the control performance. The time delay and mean absolute error (MAE) are defined to analyze the human-machine torque. The comparative results are shown in Table III. As the initial time delay of the whole exoskeleton robot is 0.01s, the PID controller acquires the time delay of 0.011 second. Meanwhile, the time delay increase under the effect of the PID controller, because their exists the inevitable rise time. On the other side, the Smith predictor controller gains the time delay of 0.001 second, and decreases the time delay deeply. Additionally, the Smith predictor controller acquires less MAE (i.e., 0.0235 N.m) than the PID controller (i.e., 0.0674 N.m). The quantitative analysis could declare that the Smith predictor controller promotes the control performance for the exoskeleton robot.

V. CONCLUSION

The dynamic model of the lower exoskeleton robot driven by EHSS is built through the fluid equation and Newton equation in this paper. For the dynamic model, the inputs are the joint angles, velocities and accelerations, while the outputs are the desired torques which indicate that how much torque the human and the machine should provide together. Meanwhile, the control aim is to reduce the torque generated by the human. To enhance the control performance, the Smith predictor is selected to compensate the time delay, and compared with the traditional PID controller. The input data are extracted from the actual sensors mounted inside the exoskeleton, and tested on the Matlab platform. The results show that the Smith predictor tremendously decreases the time delay, and promotes the control performance.

REFERENCES

[1] K. Kong, and D Jeon, "Design and control of an exoskeleton for the elderly and patients," *IEEE/ASME Transactions on Mechatronics*, vol. 11, no.4, pp428-432, 2006.
[2] D. Wang, K. M. Lee, and J. Guo, "Adaptive knee joint exoskeleton based on biological geometries," *IEEE/ASME Transactions on Mechatronics*, vol. 19, no.4, pp1268-1278, 2014.
[3] Z. Li, B. Huang, and A. Ajoudani, "Asymmetric bimanual control of dual-arm exoskeletons for human-cooperative manipulations," *IEEE Transactions on Robotics*, vol. 34, no.1, pp264-271, 2018.
[4] X. Lu, Y. Bai, and B. Fan, "A hybrid offline/online modeling based tracking control for complex hydraulic driving processes," *IEEE Access*, vol. 7, pp106102-106110, 2019.
[5] C. Lv, H Wang, and Cao. D, "High-precision hydraulic pressure control based on linear pressure-drop modulation in valve critical equilibrium state," *IEEE Transactions on Industrial Electronics*, vol. 64, no.10, pp7984-7993, 2017.
[6] A. B. Zoss, H. Kazerooni, and A Chu. "Hybrid control of the Berkeley lower extremity exoskeleton (BLEEX)," *IEEE/ASME Transactions on Mechatronics*, vol. 11, No.2, pp128-138, 2006.
[7] None. "Protonex powers lockheed Martin HULC exoskeleton," Fuel Cells Bulletin, vol.2, pp4-5, 2010.
[8] Y. Huang, D. M. Pool, and O. Stroosma, "Long-stroke hydraulic robot motion control with incremental nonlinear dynamic inversion," *IEEE/ASME Transactions on Mechatronics*, vol. 24, no.1, pp304-314, 2019.
[9] L. Yu, J. B. Zheng, Y. Wang, E. Q. Zhan and Q. Z. Song, "Direct force control for human-machine system with friction compensation," *Kybernetes*, vol. 45, no.5, pp760-771, 2016.
[10] Jian Zhang, Lie Yu, and Lei Ding, "Velocity feedback control of Swing *phase for 2-DoF robotic leg driven by electro-hydraulic servo system," Engineering Letters*, vol. 24, no.4, pp378-383, 2016.
[11] S. Giraldo, C. Rodolfo, and J. E. Normey-Rico, "A method for designing decoupled filtered Smith predictor for square MIMO systems with multiple time delays," *IEEE Transactions on Industry Applications*, vol. 54, no.6, pp6439-6449, 2018.
[12] H. Xing, J. Ploeg, and H. Nijmeijer, "Smith predictor compensating for vehicle actuator delays in cooperative ACC systems," *IEEE Transactions on Vehicular Technology*, vol. 68, no.2, pp1106-1115, 2019.
[13] F. Gao, M. Wu, J. She J, "Delay dependent guaranteed cost control based on combination of Smith predictor and equivalent input disturbance approach," *ISA Transactions*, vol. 62, pp215-221, 2016.
[14] M. Bowthorpe, M. Tavakoli, H. Becher et al, "Smith Predictor-Based Robot Control for Ultrasound-Guided Teleoperated Beating-Heart Surgery," *IEEE Journal of Biomedical and Health Informatics*, vol. 18, no.1, pp157-166, 2014.
[15] Lie Yu, Lei Ding, Qinlan Xie, and Fangli Yu, "Active Disturbance Rejection Control of Position Control for Electrohydraulic Servo System," *Engineering Letters*, vol. 28, no.3, pp944-948, 2020.
[16] H. E. Merritt, "Hydraulic control systems", John Wiley & Sons, (1967), New York.